DIRECT OBSERVATION OF THE LUNAR PHOTOELECTRON LAYER

by

David L. Reasoner

and

William J. Burke

Department of Space Science
Rice University
Houston, Texas 77001

December 1971

INTRODUCTION

The general problems of photoelectron emission by an isolated body in a vacuum and in a plasma have been the objects of several investigations. For example, Medved (1965) has treated electron sheath formations about bodies of typical satellite dimensions. Guernsey and Fu (1970) have considered the properties of an infinite, photoemitting plate immersed in a dilute plasma. Grobman and Blank (1969) obtained expressions for the lunar surface potential due to photoelectron emission while the moon is in the solar wind. Walbridge (1970) developed a set of equations for obtaining the density of photoelectrons as well as the electrostatic potential as functions of height above the surface of the moon while the moon is in the solar wind. By assuming a simplified form of the solar photon emission spectrum he could provide analytic expressions for these quantities.

In this paper we report on observations of stable photoelectron fluxes, with energies between 40 and 200 ev by the Apollo XIV Charged Particle Lunar Environment Experiment (CPLEE). These observations, made in the magnetotail under near vacuum conditions, are compared with numerically calculated photoemission spectra to determine the approximate potential difference between ground and CPLEE's apertures (26 cm). Numerically calculated density and potential distributions, when compared with our measured values, help us estimate the photoelectron yield function of the dust layer covering the moon.

We have also developed a hydrostatic model for a photoelectron gas in equilibrium above the surface of the moon. An

equation of state $P = \text{const } n^{\gamma}$ is postulated with γ kept as a free parameter to be determined from the numerical analysis.

THE INSTRUMENT

A complete description of the CPLEE instrument has been given by O'Brien and Reasoner (1971). The instrument contains two identical charged-particle analyzers, hereafter referred to as Analyzers A and B. Analyzer A looks toward the local lunar vertical, and Analyzer B looks 60° from vertical toward lunar west.

The particle analyzers contain a set of electrostatic deflection plates to separate particles according to energy and charge type, and an array of 6 channel electron multipliers for particle detection. For a fixed voltage on the deflection plates, a five band measurement of the spectrum of particles of one charge sign and a single-band measurement of particles of the opposite charge sign are made. The deflection plate voltage is stepped through a sequence of 3 voltages at both polarities, plus background and calibration levels with zero voltage on the plates. A complete measurement of the spectrum of ions and electrons with energies between 40 ev and 50 kev is made every 19.2 seconds. Of particular relevance to this study are the lowest electron energy passbands. With a deflection voltage of -35 volts, the instrument measures electrons in five ranges centered at 40, 50, 65, 90 and 200 ev. With +35 volts on the deflection plates, electrons in a single energy range between 50 and 150 ev are measured.

OBSERVATIONS

In this section we present data from the February 1971 passage of the moon through the magnetotail. Because these are so typical, the display of data from subsequent months would be redundant. At approximately 0300 UT on February 8 CPLEE passed from the dusk side magnetosheath into the tail. The five minute averaged counting rates for Analyzer A, Channel 1, at -35 volts measuring 40 ev electrons are plotted for this day in Figure 1. Almost identical count rates are observed in Analyzers A and B during this period of observation. As CPLEE moves across the magnetopause the counting rate drops from $\sim$ 200/cycle to the magnetotail photoelectron background of $\sim$ 35/cycle (1 cycle = 1.2 sec). Enhancements at $\sim$ 0530 hours and at $\sim$ 0930 hours correspond to plasma events associated with substorms on earth (Burke and Reasoner, 1971). There is a data gap from 1000 to 1200 hours. With the exception of the short lived ($\leq$ 1 hour) enhancements the detector shows a stable counting rate over the entire day.

Our contention is that these stable fluxes observed in the magnetotail during quiet times are photoelectrons generated by ultraviolet radiation from the sun striking the surface of the moon. In support of this thesis we have reproduced the counting rates observed in the same detector on February 10 when the moon was near the center of the tail (Figure 2). First, we note that the stable count level is the same at the center as it was when CPLEE first entered the tail. Secondly, from about 0500 to 1000 hours the moon was in eclipse. During this time we observe the counting rates go to zero. As the moon emerges from the earth's shadow, the counting rates

return to their pre-eclipse levels. If the stable low energy electrons were part of an ambient plasma, rather than photoelectrons, the counting rates would not be so radically altered as the moon moved across the earth's shadow.

It could be argued that the observed counting rates were due to photons scattering within the detectors themselves and not due to lunar surface photoelectrons. This however is not the case. Preflight calibrations with a laboratory ultraviolet source showed enhanced counting rates only when the angle between the look direction of the detector and the source was less than 10°. Given the 60° separation between the look directions of Analyzers A and B, it would be impossible for the sun, essentially a point source, to produce identical counting rates in both analyzers simultaneously. There are times when we do observe ultraviolet contamination in one or the other channel. An example of such contamination is shown in Figure 3 from February 11, 0600 hours to February 12, 0900 hours. As the sun moves across the aperture of Analyzer A the counting rates increase a full order of magnitude. During this period Analyzer B continued to produce typical deep tail counting rates. Note that as the detector came out of ultraviolet contamination it encountered typical magnetosheath plasma. At ~ 0345 it passed back into the magnetotail, then at ~ 0800 returned to the magnetosheath.

We also would reject any argument to the effect that the surface of the detector is the chief source of the photoelectrons. The top surface of CPLEE is covered by polished gold plating. The photoelectron yield of such a pure polished metal is between two and three orders of magnitude lower than the probable yield function of the lunar surface (Walbridge, 1970).

A typical spectrum of photoelectrons shown in Figure 4 was observed by Analyzer A at ~ 0400 hours on February 10, shortly before the moon entered penumbral eclipse. The dark line marks the differential flux equivalent to a background count of one per cycle in each channel. For all five channels, with the deflection plates at -35 volts, the differential flux is well above this background level. During geomagnetically quiet times no statistically significant counts are observed when the deflection plates are at -350 or -3500 volts corresponding to electrons with E > 500 ev (Burke and Reasoner, 1971).

With the exception of periods of ultraviolet contamination in Analyzer A, we always observe nearly the same counting rate due to photoelectrons in Analyzers A and B. For all purposes, we can say that the spectrum displayed in Figure 4 is just as typical as for Analyzer B. We have found no case of anisotropy in the photoelectron fluxes. In all cases too, we found that the photoelectron spectra observed in both analyzers were close to a power low dependence on energy. If we write the differential flux in the form $j(E) = j_o(E/E_o)^{-K}$ where K is between 3.5 and 4, $E_o = 40$ ev and $j_o \sim 3 \times 10^5$ electrons/cm^2-sec-ster-ev. In the following section the details of this spectrum are more carefully studied.

Also in Figure 4 we display a schematic cross section of our instrument as it is deployed on the surface of the moon. The apertures of both analyzers are elevated 26 cm from ground. Their geometry is such that they observe only electrons with a component of velocity in the downward direction. Since we continually observe photoelectrons with energies up to ~ 200 ev,

we must assume that the lunar surface potential on the order of 200 volts during these times. This measurement will seem high to those familiar with the work of Walbridge (1970) and Grobman and Blank (1969), who calculate a surface potential that is at least an order of magnitude lower. The difference is that their models deal with photoemissions from the surface of the moon in the presence of the solar wind. Our measurements in the magnetotail are made under near-vacuum conditions. After further analysis of the problem we return to considerations of the surface potential.

To summarize: During geomagnetically quiet times, when the moon is in the magnetotail and not in eclipse, stable photoelectron fluxes with energies between 40 and 200 ev are observed. These fluxes are isotropic and obey a power law, E^{-K}, where K is between 3.5 and 4. From the fact that CPLEE is observing downward moving electrons we conclude that in the magnetotail the lunar surface potential is on the order of 200 volts.

A HYDROSTATIC MODEL

Our observation of steady photoelectron fluxes that are isotropic over the lower half plane for much of the moon's passage through the magnetotail suggests that we can make the following assumptions about the physical situation:

(1) The solar radiation flux at, as well as the photoelectron produced by, the lunar surface are constant in time.

(2) There are equal probabilities for emitting photoelectrons into equal solid angle elements in the upper half plane.

(3) In the equilibrium situation the net current out of the surface is zero.

(4) The lunar surface may be approximated by a flat infinite plane. Physical quantities vary only with height above the surface. (The coordinate system is such that X, Y, Z increase toward the local vertical, west and south respectively.)

The first assumption assures a constant flux of photoelectrons at the surface of the moon. In Appendix A we show that our postulation of an isotropic production of photoelectrons is sufficient to explain our observation of isotropic fluxes at 26 cm. Assumption three demands that in the vacuum case all photoelectrons are trapped by the electrostatic field above the surface. The surface potential under vacuum conditions is determined by the most energetic photoelectrons.

In the equilibrium situation the governing equations are:

$$\frac{\partial^2 \Phi(x)}{\partial x^2} = -4\pi q n(x) \qquad \text{Poisson's Equation} \qquad (1)$$

$$q \frac{\partial \Phi(x)}{\partial x} = + \frac{1}{n(x)} \frac{\partial P(x)}{\partial x} \qquad \text{Conservation of Momentum} \qquad (2)$$

Here the density and pressure are defined by

$$n(x) = \int f(\vec{v},x) d^3v$$

and

$$P(x) = \int mv^2 f(\vec{v},x) d^3v$$

The density can be eliminated from equations (1) and (2) to show that

$$P(x) = \frac{1}{8\pi} \left(\frac{\partial \Phi(x)}{\partial x} \right)^2$$

However to solve for all three quantities we must postulate an equation of state

$$\frac{P(x)}{n^\gamma(x)} = \frac{P_o}{n_o^\gamma} = \alpha \qquad (3)$$

α is a constant and γ is related to the polytrope index ν by the relationship $\gamma = (\nu + 1)/\nu$. The values of physical quantities at the surface are denoted by zero subscripts. In solving equations (1) - (3) we demand that as $x \to \infty$ all physical quantities go to zero.

Pressure can be eliminated by differentiating equation (3) and substitution into (2).

$$\frac{\partial \Phi}{\partial x} = + \frac{\gamma \alpha}{q} \; n^{\gamma-2} \; \frac{dn}{dx} \tag{4}$$

If we multiply (1) by $\frac{\partial \Phi}{\partial x}$, using (4) on the right hand side, and integrate in from infinity, we get

$$\left(\frac{\partial \Phi}{\partial x}\right)^2 = - \; 8\pi\gamma\alpha \int_x^\infty n(x')^{\gamma-1} \frac{dn(x')}{dx'} \; dx'$$

$$\frac{\partial \Phi(x)}{\partial x} = \pm \sqrt{8\pi\alpha n^\gamma(x)} \tag{5}$$

In order to insure a potential that decreases as x increases we must choose the (-) sign in equation (5). Equating the right hand sides of equations (4) and (5)

$$- \frac{\gamma\alpha}{q} \; n^{\gamma-2} \; \frac{dn}{dx} = \sqrt{8\pi\alpha} \; n^{\gamma/2}$$

or

$$- x = \frac{\gamma}{q} \sqrt{\frac{\alpha}{8\pi}} \int_{n_o}^{n(x)} n^{\frac{\gamma}{2} - 2} \; dn$$

For $\gamma \neq 2$

$$n(x) = n_o \left[1 - \frac{\gamma-2}{\gamma} \; \frac{x}{\lambda}\right]^{\frac{2}{\gamma-2}} \tag{6a}$$

and for $\gamma = 2$

$$n(x) = n_o e^{-x/\lambda}$$

with

$$\lambda = \sqrt{P_o/2\pi q^2 n_o^2} \quad . \tag{6b}$$

Equations (6a) and 6b) may be substituted into (4) to get:

$$\Phi_o - \Phi(x) = \frac{2P_o}{\lambda q n_o} \int_o^x \left(1 - \frac{\gamma-2}{\gamma} \frac{x}{\lambda}\right)^{\frac{\gamma}{\gamma-2}} dx, \quad \gamma \neq 2 \tag{7a}$$

$$\Phi_o - \Phi(x) = \frac{2P_o}{qn_o} (1 - e^{-x/\lambda}) = -\frac{P_o \gamma}{qn_o} (1 - e^{-x/\lambda}) \quad \gamma = 2 \tag{7b}$$

The $\gamma \neq 2$ case, (7a) has two formal solutions depending on whether γ equals 1 or not.

$$\Phi_o - \Phi(x) = \frac{P_o \gamma}{qn_o(\gamma-1)} \left[1 - \left\{1 - \frac{\gamma-2}{\gamma} \frac{x}{\lambda}\right\}^{\frac{2(\gamma-1)}{\gamma-2}}\right], \gamma \neq 1,2 \tag{7a'}$$

and

$$\Phi_o - \Phi(x) = \frac{2P_o}{qn_o} \ln\left(1 + \frac{x}{\lambda}\right); \quad \gamma = 1 \tag{7a''}$$

The solutions for the electrostatic potential, equations (7a') and (7a'') and (7b) satisfy the boundary conditions

$\Phi(0) = \Phi_o \approx 200$ volts and $\Phi(\infty) = 0$. Here $\Phi_o = \frac{P_o}{qn_o} \frac{\gamma}{\gamma-1}$.
If $1 < \gamma \leq 2$, $\Phi(x)$ goes smoothly to zero as $x \to \infty$. If $\gamma = 2$, $\Phi(x)$ goes to zero at $x = \frac{\lambda \gamma}{\gamma-2}$. However of $0 < \gamma \leq 1$ both boundary conditions cannot be satisfied for finite Φ_o.
It would be possible to have an equation of state with finite Φ_o and $\gamma \leq 1$ near the surface, but the value of γ must shift to a value greater than 1 beyond some height. The numerical analysis of the following section shows that this is the case.

NUMERICAL ANALYSIS

(a) General Theory

The variations of photoelectron density and electrostatic potential above the surface of the moon can be calculated numerically. Again we approximate the lunar surface by an infinite plane, with the x direction normal to the surface, and assume spatial variations of physical quantities only with height.

At a height x above the surface the electron density is $\int f(\vec{v},x)d^3v$. $f(\vec{v},x)$ is the electron distribution function. In Appendix A we have shown that if we assume an isotropic flux at the surface, the distribution function is independent of angles at all heights. Writing $d^3v = \sqrt{\frac{2E}{m^3}}\, dE\, d\Omega$ and integrating over solid angles, the density is

$$n(x) = 4\pi \int_{\circ}^{\infty} \sqrt{\frac{2E}{m^3}}\, f(E,x)\, dE \qquad (8)$$

Since the distribution function is a constant along particle trajectories, $f(E,x) = f(E_o,x = 0)$. Where $E = E_o - q[\varphi_o - \varphi(x)]$. By changing the variable of integration from E to E_o equation (8) can be expressed

$$n(x) = 4\pi \int_{q[\varphi_o-\varphi(x)]}^{\infty} \sqrt{2m(E_o-q[\varphi_o-\varphi(x)])}\, f(E_o,x = 0)\, dE_o \qquad (9)$$

To calculate the distribution function of photoelectrons at the surface consider the quantity

$$j(E_o)dE_o = \left[\int_W^\infty I(h\nu)Y(h\nu)\rho(E_o,h\nu)dh\nu \right] dE_o \qquad (10)$$

the upward moving flux of photoelectrons emitted from the surface with energies between E_o and $E_o + dE_o$. $I(h\nu)d(h\nu)$ is the flux of photons reaching the lunar surface with energies between $h\nu$ and $h\nu + d(h\nu)$. $Y(h\nu)$, the quantum yield function, gives the number of electrons emitted by the surface per incident photon with energy $h\nu$. $\rho(E_o,h\nu)dE_o$ is the probability that an electron emitted from the surface, due to a photon with energy $h\nu$, will have a kinetic energy between E_o and $E_o + dE_o$. $\rho(E_o,h\nu)$ is normalized so that

$$\int_o^\infty \rho(E_o,h\nu)dE_o = 1.$$

W is the work function of the lunar surface material.

The total upward moving flux at the surface is $S_\uparrow(x = 0) = \int_o^\infty j(E_o)dE_o$. But

$$S_\uparrow(x = 0) = \int_o^{2\pi} \int_o^{\pi/2} \int_o^\infty \vec{v}_o \, f(E_o,\theta,\varphi,0)v_o^2 \, dv_o \cdot \sin\theta \, d\theta \, d\varphi.$$

Since $\vec{v}_o = v_o[i \cos\theta + j \sin\theta \cos\varphi + k \sin\theta \sin\varphi]$ and f is independent of angle

$$S(x = 0) = \pi \int_o^\infty \frac{2E_o}{m^2} f(E_o,x = 0)dE_o \qquad (11)$$

Thus

$$f(E_o, x = 0) = \frac{m^2 \, j(E_o)}{2\pi \, E_o} \tag{12}$$

and

$$n(x) = 2 \int_{q[\varphi_o - \varphi(x)]}^{\infty} \frac{\sqrt{2m(E_o - q[\varphi_o - \varphi(x)])}}{E_o} \, j(E_o) \, dE_o \tag{13}$$

The potential as a function of height is evaluated by multiplying eq. (1) [Poisson's Equation] by $\partial\varphi/\partial x$ and integrating in from $x = \infty$ to get

$$\left(\frac{d\varphi}{dx}\right)^2 = - 8\pi q \int_{\varphi(x)}^{o} n(\varphi') \, d\varphi' \tag{14}$$

where we have written $\int_x^{\infty} n(x') \frac{d\varphi}{dx}, \, dx' = \int_{\varphi(x)}^{o} n(\varphi') d\varphi'$. A further integration out from the surface, gives us the potential at a point x.

(b) Computational Methods and Results

To determine the upward moving differential flux at the surface, upon the knowledge of which the distribution function, number density and potential depend, we must first solve the integral in equation (10). The solar photon differential flux at 1 A.U., $I(h\nu)$, is taken from Friedman (1963) for the range

2000 to 1800 Å and from Hinteregger (1965) for the range 1775 - 1 Å and is plotted in Figure (5). Following the suggestion of Walbridge (1970) we have:

(1) Adopted a work function of lunar material of 6 ev.

(2) Assumed a photoelectron yield function of the form

$$Y(h\nu) = \begin{cases} u(h\nu-6)\, Y_o \dfrac{h\nu-6}{3} & h\nu < 9 \text{ ev} \\ Y_o & h\nu > 9 \text{ ev} \end{cases} \qquad (15)$$

where $u(h\nu)$ is a unit step function and Y_o is a free parameter of our calculation.

(3) Chosen a probability function

$$\rho(E,h\nu) = \begin{cases} 6E(E_1-E)/E_1 & 0 \le E \le E_1 \\ 0 & E > E_1 \end{cases} \qquad (16)$$

where

$$E_1 = \begin{cases} h\nu-W & h\nu \ge W \\ 0 & h\nu < W \end{cases}$$

In general the probability function is a complicated function depending on the nature of the photoemission material. However, Grobman and Blank (1968) have shown that for the purpose of calculating equation (10) any broad function with zeros at $E = 0$ and $E = E_1$ and a width $\Delta E \sim h\nu$ will suffice. A plot of $\rho(E,h\nu)$ is shown in Figure 6 for various values of E_1.

The upward directed differential flux in electrons/cm^2-sec-ster-ev for the values $Y_o = 1, .1, .01$ were numerically

computed and have been plotted in Figure (7). We have also inserted the photoelectron differential flux observed by CPLEE at 26 cm. The Liouville theorem shows us to set a lower bound on Y_o of .1. That is if there were no potential difference between the ground and 26 cm the yield function would be .1 electrons/photon . After estimating the potential difference between 26 cm and ground we can also determine an upper bound on Y_o.

Solving the integro-differential equation (14) for $\varphi(x)$ involves an integration from the surface outward, with an assumed value of φ_o. However the expression for $\partial\varphi/\partial x$ involves an integral from infinity in to x, or equivalently from $\varphi = 0$ to $\varphi(x)$. Integrals of this type are ordinarily impossible to evaluate numerically. By the expedient of dividing the integral into pieces in E_o space and using an analytic approximation to the function $j(E_o)$ in each of these intervals, a solution was effected. In this way it was only necessary to know the values of $\varphi = \varphi(x)$ and $\varphi = 0$ at the end points of the interval, and the solution would proceed. In Figure (10) we show families of solutions for $\varphi(x)$ with several values of the parameter Y_o.

The value of Y_o calculated by assuming no potential difference between the surface and x = 26 cm was 0.1. Figure (8) shows that for $Y_o = 0.1$, the potential difference $\Phi(x=0) - \Phi(x=26\ cm)$ is only 3 volts. Obviously, we could now use an iterative procedure, modifying our spectral measurement at 26 cm to obtain the surface spectrum according to the equation $f(E,x) = f(E_o,0)$ and hence obtain a new estimate of Y_o. However, the procedure is hardly justified considering the small potential difference ($\sim$ 3 volts) and the energy range of the

measured photoelectrons (40-200 ev). Hence we conclude from our numerical analysis and measured photoelectron fluxes a lunar surface potential on the order of 200 volts and a value of the average photoelectron yield of Y_o = 0.1 electrons/ photon.

THE LUNAR SURFACE POTENTIAL φ_o

The solar photon energy spectrum (Figure 5) shows a marked decrease at $h\nu$ = 200 ev. For the case of the moon in a vacuum the potential of the lunar surface would be equal to the highest energy photon present minus the lunar surface work function. Hence we estimate the lunar surface potential φ_o to be 200 volts. This is confirmed by the experimental measurements, as the photoelectron energy spectrum shows a measurable flux at 200 ev but no significant flux in the next highest energy channel at 500 ev.

The lunar surface potential can be decreased however by the presence of a hot ambient plasma which can furnish an electron return current which can partially balance the emitted photoelectron current. In effect, the highest energy photoelectrons can escape from the potential well, since electrons from the ambient plasma furnish the return current to balance these escaping photoelectrons. Quantitatively, if F_s is the net negative flux to the lunar surface from the ambient plasma, and $j(E_o)$ is the emitted photoelectron energy spectrum in units of electrons/cm^2-sec, then:

$$F_s = \int_{-q\varphi_o}^{\infty} j(E_o)\,dE_o$$

and this equation can be solved for φ_o, the lunar surface potential.

Our measurements of photoelectrons were taken during periods in the magnetotail when all of the channels of the instrument except the lowest-energy electron channels were at

background levels. Thus we can establish an upper limit to the electron flux from the ambient plasma for electrons with 40 ev < E < 50 kev. Figure 4 shows the "background spectrum", calculated by converting the background counting rate of ~ 1 count/second to equivalent flux in each of the energy channels. Integrating over this spectrum and converting to omnidirectional flux over the hemisphere gives $F_s \leq 3.4 \times 10^6$ electrons/cm^2-sec. We feel that this is a valid upper limit, as the range of measurement in energy includes both the peak energy of the plasma sheet spectrum (~ 1 kev) and of the magnetosheath spectrum (~ 40-60 ev).

We note that Vasyliunas (1968) obtained an upper limit to the electron concentration for locations outside of the plasma sheet based on OGO-3 data. The relation expressed was $NE_o^{\frac{1}{2}} < 10^{-2}$ cm^{-3} kev$^{\frac{1}{2}}$ where N is the electron density and E_o is the energy at the peak of the spectrum. For an isotropic plasma where the bulk motion can be neglected relative to the thermal motion, the electron flux to a probe is given by $F_s = N\bar{v}/2\sqrt{\pi}$. Applying the appropriate conversion of factors, the expression of Vasyliunas results in an upper limit to the electron flux of $F_s < 5.6 \times 10^7$ electrons/cm^2-sec.

The emitted photoelectron energy spectrum $j(E_o)$ is shown in Figure 6. The procedure involved in calculating the surface potential φ_o is to integrate the function $j(E)$ from the maximum energy of 200 ev backwards until the total flux is equal to the upper limit of the return flux. The computation was done for Y_o = 1, .1, and .01, and for the two values of the upper limit of the return flux derived above. The results are shown in Table 1.

TABLE 1

Electron Flux	Y_o	Φ_o (volts)
3.4×10^6	.01	181
3.4×10^6	.1	114
3.4×10^6	1	44
5.6×10^7	.01	96
5.6×10^7	.1	36
5.6×10^7	1	8

The lower half-height of the Channel 5 energy passband is 160 ev. Hence the surface potential could be as low as 160 volts and still result in particle fluxes in Channel 5. This estimate of the potential is seen to be not inconsistent with a value of $Y_o = 0.1$, $F_s \leq 3.4 \times 10^6$ resulting in a surface potential (Table 1) of 114 volts.

DISCUSSION

For the sake of comparison with the predictions of the hydrostatic model, we have plotted the numerically calculated density, pressure and potential difference from $x = 0$ out to a height of 200 meters in Figure 9. In Figure 10 the pressure is plotted as a function of number density to obtain the equation of state. We find that from $0 < x \leq 30$ cm, the value of $\gamma \approx 0.5$. From 30 to 100 cm γ drops to a value of 0.2 then recovers to about 0.5 out to $x = 2000$ cm. Beyond this point γ shifts toward a value greater than 1.

The dashed lines in Figure 8 represent the density and potential difference as computed from equations 6a and 7a' using $\gamma = .5$. A surface pressure of $\sim 2 \times 10^{-8}$ ergs/cm^3 and density $\sim 6 \times 10^4$ cm^{-3} give a value of $\lambda = 2.1$ cm. Out to x=200 cm the numerically calculated potential agrees quite well with the hydrostatic prediction. Beyond this height the potential difference rises less steeply than the $\gamma = .5$ prediction. However this can be understood in terms of the shift to larger than unity values of γ required by equation 7a' if the boundary condition $\Phi(\infty) = 0$ is to be met.

The density curve is much more sensitive to fluctuations in the value of γ. It is interesting to note that the variations in the region $30 \leq x \leq 300$ cm correspond to potential differences of 3 to 15 volts from ground. We note that in Figure 9 the photoelectron flux generated at the surface has sharp breaks in this region. Evidently the photoelectrons can be broken up into three groups of low ($0 < E \leq 1$ ev), medium ($1 < E < 10$ ev) and high ($10 < E < 200$ ev) energy. Where one

distribution dominates over the others a value of γ is established. Fluctuations in γ are found in the transition regions between populations.

SUMMARY AND CONCLUSIONS

In this paper we have reported the observation of stable, isotropic photoelectron fluxes 26 cm above the lunar surface. In the energy range $40 \leq E \leq 200$ the flux obeys a power law of the form $j(E) = j_o(E/E_o)^{-K}$ where K is between 3.5 and 4, $j_o = 2 \times 10^5$ electrons/cm^2-ster-sec-ev, and $E_o = 40$ ev. Because these fluxes were moving down we conclude that in the near vacuum conditions of the high latitude magnetotail the lunar surface potential is at least 200 volts. It was shown that these electrons can be explained in terms of the measured solar photon spectrum producing an isotropic flux of photoelectrons at the surface. A photoelectron yield function of $Y_o = 0.1$ electron/photon was calculated. Finally, we have shown that the numerically calculated pressure, density and potential distributions can be approximated by the solutions to a set of hydrostatic equations that employs an equation of state $P/n^{\frac{1}{2}} = \text{const}$ out to 200 cm from the surface. Beyond this height the equation of state shifts toward the isothermal case, $P/n = \text{const}$.

APPENDIX A

Here we present a justification for using a scalar pressure in the equation of state [equation (3)].

By definition the number density, flux and pressure are

$$n(x) = \int f(\vec{v},x)\,d^3v = \int N(E,\Omega,X)\,dE\,d\Omega$$

$$\vec{S}(x) = \int \vec{v}\, f(\vec{v},x)\,d^3v = \int v\, S(E,\Omega,X)\,dE\,d\Omega \qquad \text{(A-1)}$$

$$P(x) = \int m\vec{v}\vec{v}\, f(\vec{v},x)\,d^3v = \int vv\, P(E,\Omega,X)\,dE\,d\Omega$$

Here we have used $d^3v = v^2 dv \sin\theta\, d\theta\, d\Phi = \sqrt{\frac{2E}{m^3}}\, dE\, d\Omega$ and defined the directional differential density, flux and pressure

$$N(E,\Omega,\ ) \equiv \left(\frac{2E}{m^3}\right)^{\frac{1}{2}} f(E,\Omega,X)$$

$$S(E,\Omega,X) \equiv \frac{2E}{m^2} f(E,\Omega,X) \qquad \text{(A-2)}$$

$$P(E,\Omega,X) \equiv \left(\frac{2E}{m}\right)^{3/2} f(E,\Omega,X)$$

The angular dependence of these quantities is contained only in the distribution function. To compare one of the directional differential quantities at a point X_1 with its value at the ground, $X = 0$, we use the Liouville Theorem

$$f_1(E_1,\Omega_1,X_1) = f_0(E_0,\Omega_0,X_0 = 0).$$

The distribution function is a constant along particle trajectories. Subscripts 0 and 1 indicate the value of the quantity X_1 and $x = 0$.

In our model we assumed an isotropic photoelectron production (at $X = 0$) over the upper half plane in velocity space. Since all electrons are trapped in a conservative field, isotropy is maintained over the whole of velocity space at $X = 0$. Thus f_0 is independent of Ω_0. From the conservation of energy

$$E_0 = E_1 + q\left[\Phi_o - \Phi(x)\right]$$

or

$$f_1(E_1, \Omega_1, X_1) = f_o(E_1 + q\left[\Phi_o - \Phi(x)\right] \qquad \text{(A-3)}$$

Thus if photoelectrons are isotropic at the ground, they are isotropic at X. This explains our observation of isotropic fluxes, measured at $X = 26$ cm. In this case the directional differential pressure is also isotropic, and on integration reduces to the scalar form used in the text.

Being independent of angle, the distribution function is an even function about $v_x = 0$, $v_y = 0$ and $v_z = 0$. The Vlasov equation

$$\frac{\partial f}{\partial t} + v_x \frac{\partial f}{\partial x} - \frac{e}{m} \frac{\partial \Phi}{\partial x} \frac{\partial f}{\partial v_x} = 0$$

has non-trivial moment solutions only when multiplied by v_x. v_x^3, $v_x v_y^2$ or $v_x v_z^2$. These moment equations take the form

$$\frac{\partial}{\partial x} n(x) < V^2(x) > + \frac{e}{m} \frac{\partial \Phi}{\partial x} n(x) = 0 \qquad \text{(A-4)}$$

and

$$\frac{\partial}{\partial x} n < v_x^2(x) v_y^2(x) > + \frac{3e}{m} \frac{\partial \Phi}{\partial x} n(x) < v_x^2(x) > = 0$$

$$\frac{\partial}{\partial x} n < v_x^2(x) v_y^2(x) > + \frac{e}{m} \frac{\partial \Phi}{\partial x} n(x) < v_x^2(x) > = 0 \quad \text{(A-5)}$$

$$\frac{\partial}{\partial x} n < v_x^2(x) v_y^2(x) > + \frac{e}{m} \frac{\partial \Phi}{\partial x} n(x) < v_x^2(x) > = 0$$

where $n(x) < v_i^{\nu}(x) > = \int d^3v \; v_i^{\nu} \; f(v,x)$.

Since the distribution function depends only on velocity, equations (A-4) and (A-5) can be written

$$\frac{\partial}{\partial x} I_4(x) + \frac{3e}{m} \frac{\partial \Phi}{\partial x} I_2(x) = 0 \quad \text{(A-4')}$$

$$\frac{\partial}{\partial x} I_6(x) + \frac{5e}{m} \frac{\partial \Phi}{\partial x} I_4(x) = 0 \quad \text{(A-5')}$$

where $I_{2\nu}(x) = \int_0^{\infty} v^{2\nu} \; f(v,f) \; dv$.

If, for example, we had a locally Maxwellian gas

$$f(\nu,x) = \frac{n(x)}{\pi^{3/2} w^3(x)} \; e^{-v^2/w^2(x)}$$

then

$$I_{2\mu} = \frac{(2\mu-1)!!\, n(x) w(x)^{2\nu-2}}{2^{x+1}\pi}$$

and (A-4') becomes

$$\frac{\partial n(x)w^2(x)}{\partial x} + \frac{2e}{m}\frac{\partial \Phi}{\partial x} n(x) = 0$$

and (A-5')

$$\frac{\partial n(x)w^4(x)}{\partial x} + \frac{2e}{m}\frac{\partial \Phi}{\partial x} n(x)w^2 = 0.$$

Expanding we get

$$w^2(x)\left[\frac{\partial n(x)w^4(x)}{\partial x} + \frac{2e}{m}\frac{\partial \Phi}{\partial x} n(x)\right] + \eta(x)w^2(x)\frac{\partial w^2(x)}{\partial x} = 0.$$

Since the bracketed term is zero and $n(x)w^2(x) > 0$, $w^2(x)$ is a constant. This is the isothermal case, whose solution $n(x) = m_o e^{-q(\Phi_o - \Phi(x)/mw^2}$ is well known.

In general however (A-4') and (A-5') cannot be solved without assuming a distribution function, from which the equation of state may be determined from (A-5').

ACKNOWLEDGEMENTS

We gratefully acknowledge the assistance of Wayne Vogel and Patricia Moore who developed the computer programs used in the analysis.

This work was supported by National Aeronautics and Space Administration Contract No. NAS9-5884.

REFERENCES

Burke, W. J. and D. L. Reasoner, Absence of the Plasma Sheet at Lunar Distance during Geomagnetically Quiet Times, Planet. and Space Sci. (To be published), 1972.

Friedman, H., Rocket Spectroscopy, in Space Science, ed. by D. P. LeGallet, P. 549, John Wiley & Sons, New York, 1963.

Geurnsey, R. L. and J. H. M. Fu, Potential Distribution Surrounding a Photo-Emitting Plate in a Dilute Plasma, J. Geophys. Res., 75, 3193, 1970.

Grobman, W. D. and J. L. Blank, Electrostatic Potential Distribution of Sunlit Lunar Surface, J. Geophys. Res., 74, 3943, 1969.

Hinteregger, H. E., L. A. Hall and G. Schmidtke, Solar XUV Radiation and Neutral Particle Distribution in July 1965 Thermosphere, in Space Research V, ed. by D. K. King-Hele, P. Muller and G. Righini, p.p. 1175-1190, North Holland Publishing Co., Amsterdam, 1965.

Medved, D. B., On the Formation of Satellite Electron Sheaths Resulting from Secondary Emission and Photoeffects, in Interaction of Space Vehicles with an Ionized Atmosphere, ed. by S. F. Singer, p. 305, Pergamon Press, Oxford 1968.

O'Brien, B. J., and D. L. Reasoner, Charged Particle Lunar Environment Experiment, Apollo 14 Preliminary Science Report, NASA SP-272, 193, 1971.

Walbridge, E., The Lunar Photoelectron Layer I. The Steady State, (Preprint), 1970.

FIGURE CAPTIONS

1. 5 minute averaged counting rates for CPLEE, Analyzer A, Channel 1 at -35 volts, measuring 40 ev electrons on February 8, 1971. After 0300 U.T. counting rates fell from high magnetosheaths to stable photoelectron levels.

2. 5 minute averaged deep tail counting rates of 40 ev electrons on February 10, 1971. The lunar eclipse (0500 - 0900 U.T.) is marked by vanishing photoelectron counting rates.

3. An example of ultraviolet contamination of Analyzer A from $\sim$ 1200 of February 11 to $\sim$ 0300 of February 12, 1971.

4. Typical photoelectron spectrum observed by CPLEE at the lunar surface in the high latitude magnetotail.

5. Solar photon energy spectrum at 1 A.U. from 2000 to 1 Å.

6. Probability function that a photon of energy $h\nu$ will cause the lunar surface material to emit a photoelectron of energy E, with different values of $E_1 = h\nu - w$.

7. Numerically computed photoelectron spectra emitted for the yield functions $Y_o = 1$, 0.1 and .01 electrons per photon. The photoelectron spectrum measured by CPLEE is found to fall close to the $Y_o = 0.1$ line.

8. Numerically computed potential distribution above the lunar surface for several values of the yield function Y_o. For $Y_o = 0.1$ the potential difference between ground and 26 cm is about 3 volts.

9. Numerically computed values of electron density, potential difference from the surface and pressure from the surface and pressure out to 200 meters. The dashed lines represent hydrostatic solutions with $\gamma = \frac{1}{2}$.

10. Plot of photoelectron pressure against density to determine the local equation of state.

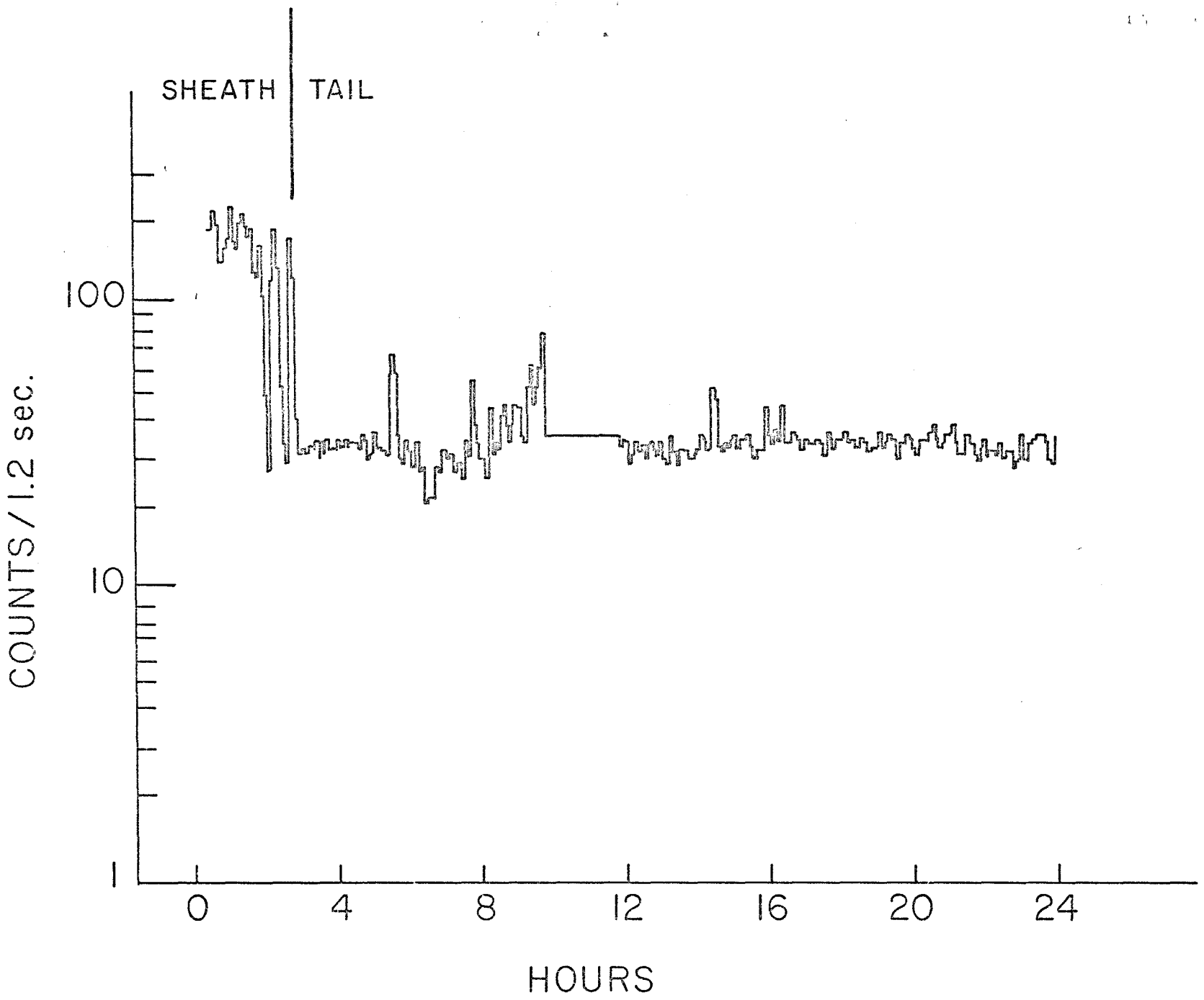

FIGURE 1

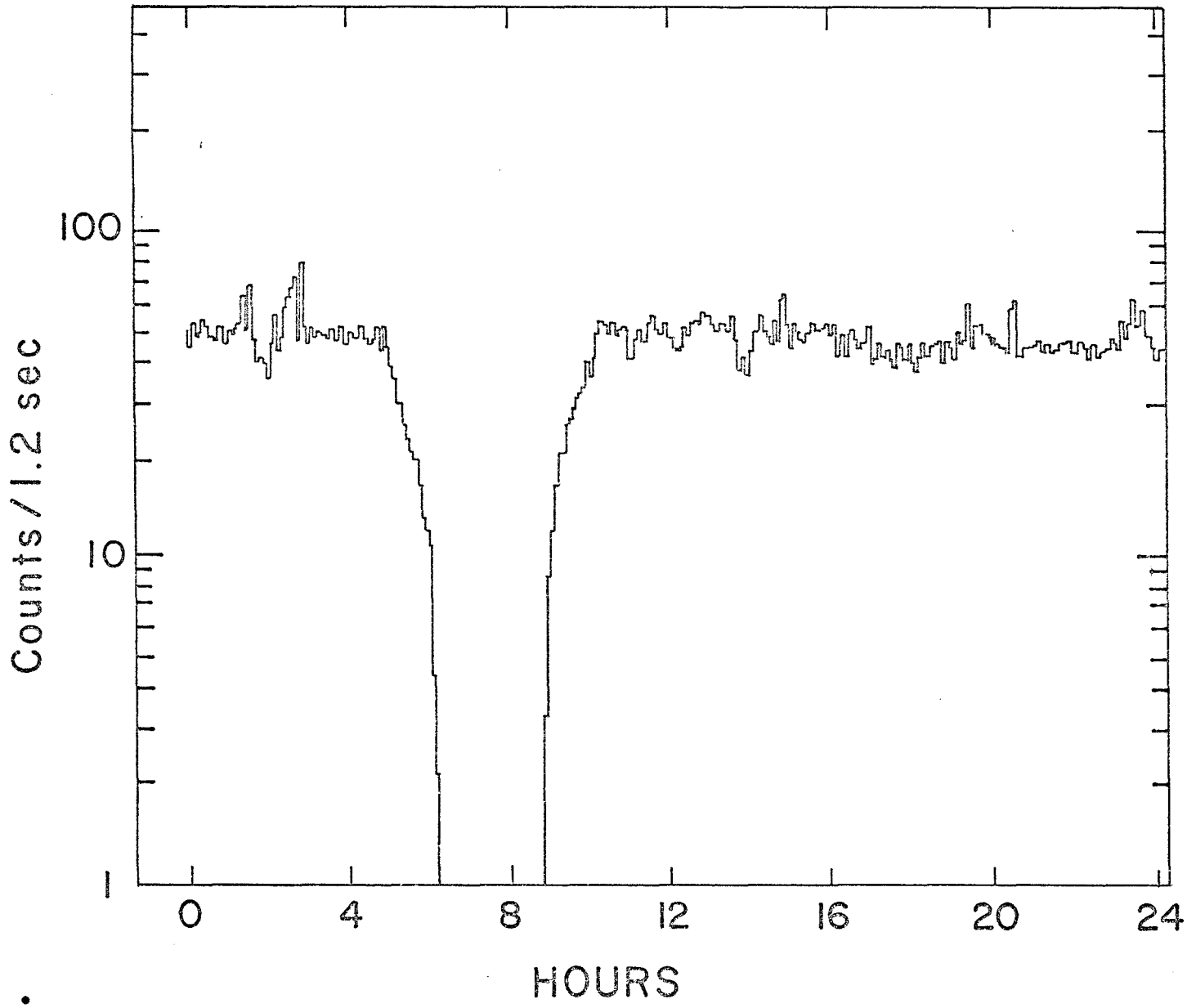

FIGURE 2

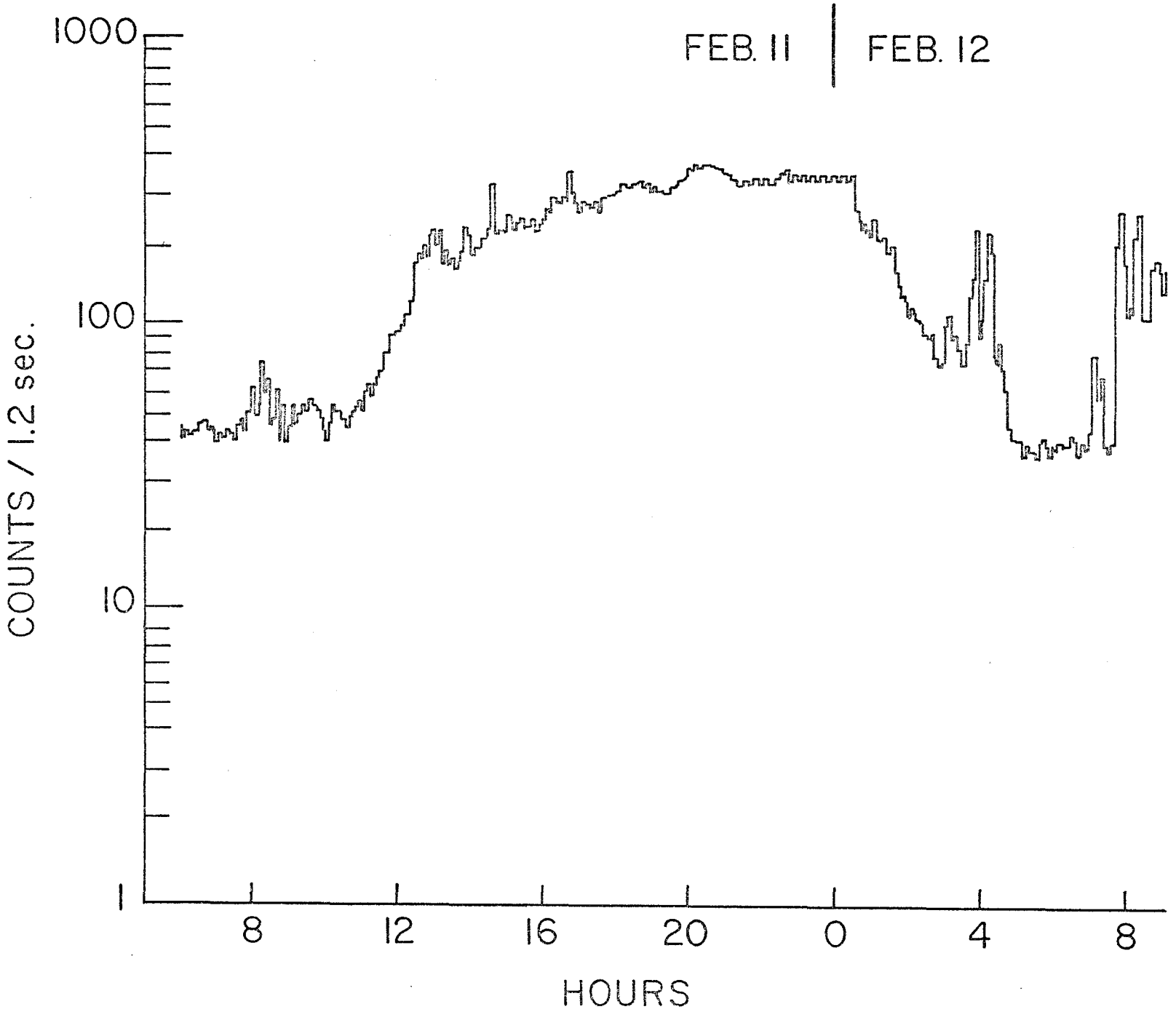

FIGURE 3

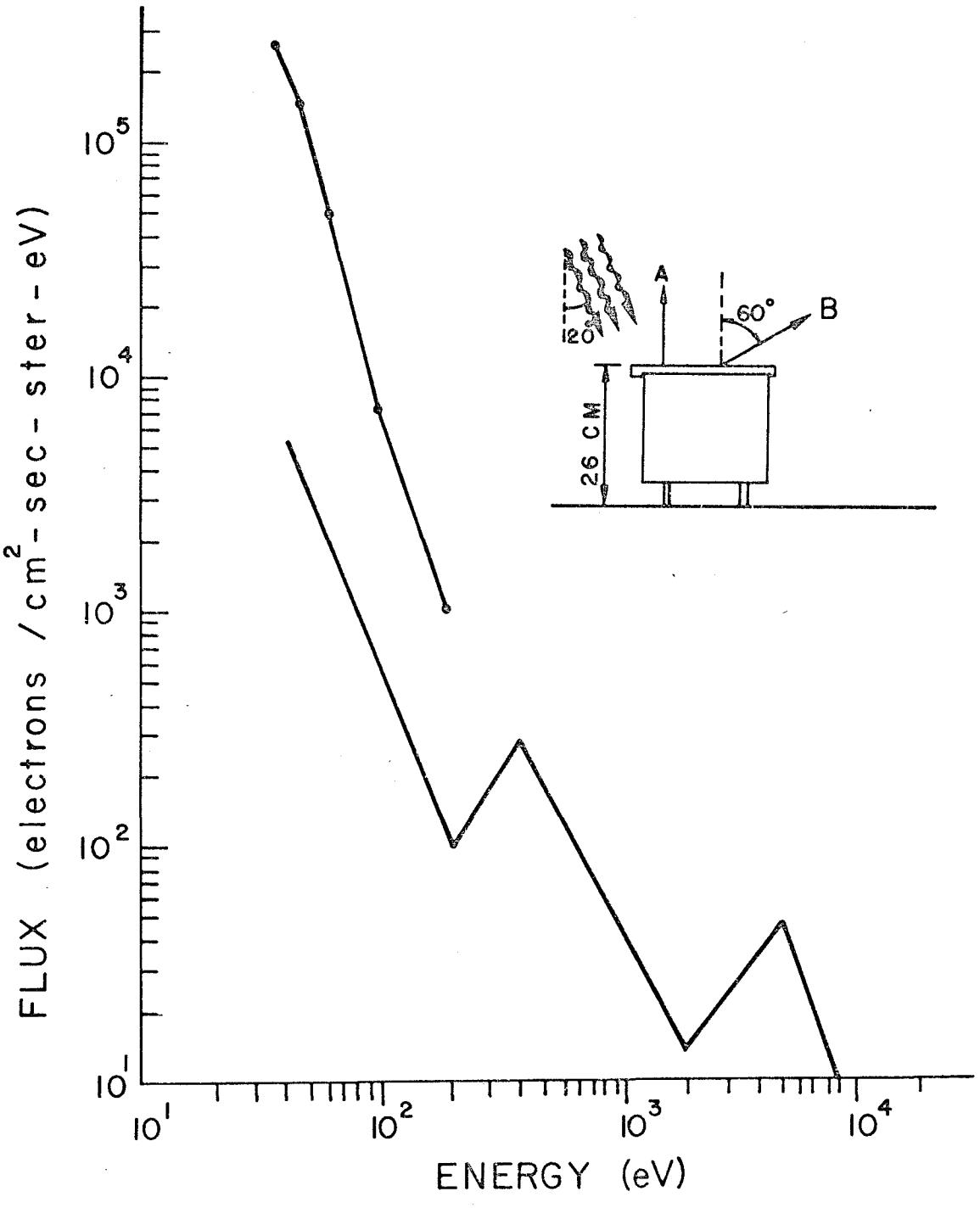
FLUX (electrons /cm^2-sec-ster-eV)
10^5
10^4
10^3
10^2
10^1
10^1
10^2
10^3
10^4
ENERGY (eV)
A
B
60°
20°
26 CM

FIGURE 4

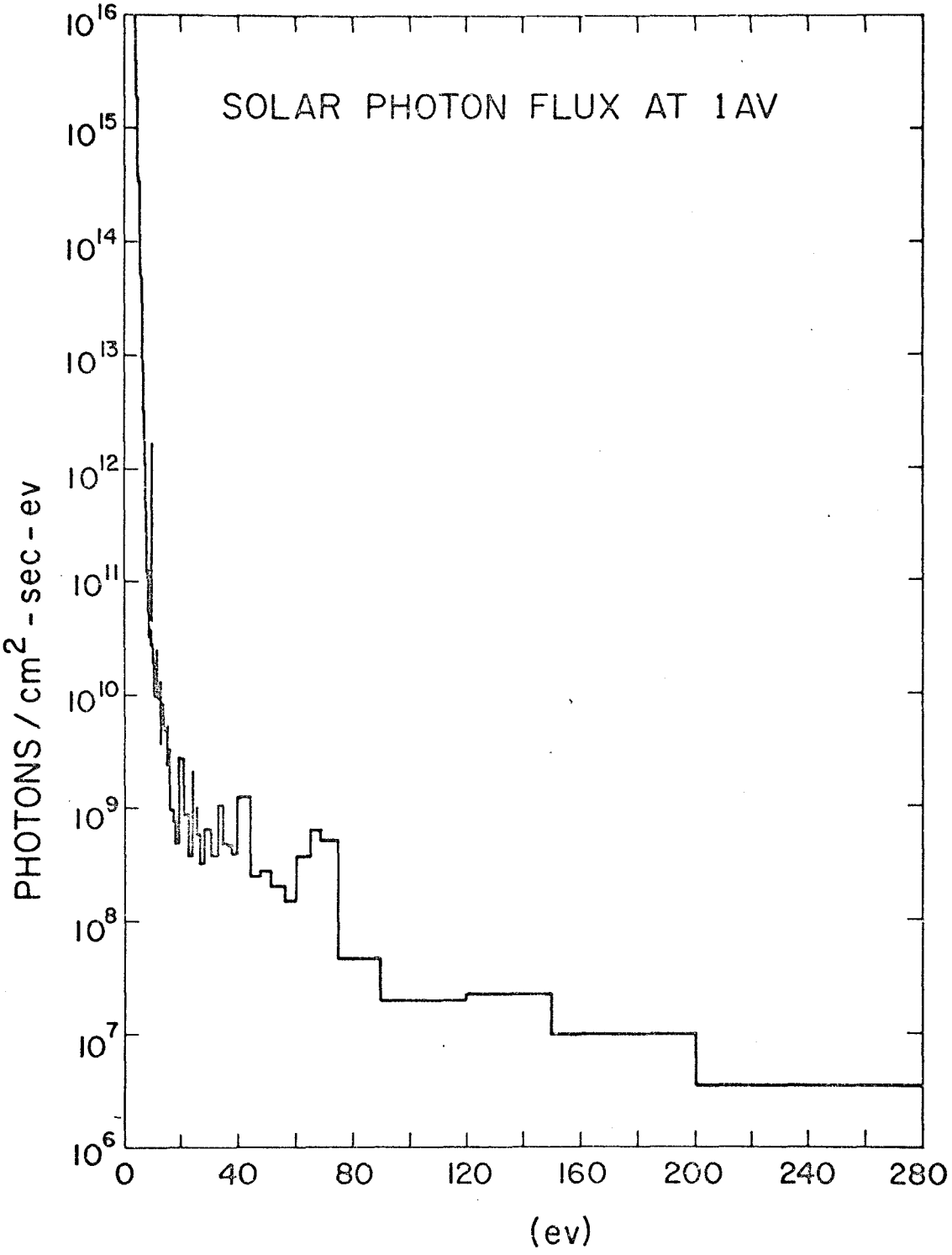
SOLAR PHOTON FLUX AT 1AV
PHOTONS / cm² - sec - ev
10¹⁶
10¹⁵
10¹⁴
10¹³
10¹²
10¹¹
10¹⁰
10⁹
10⁸
10⁷
10⁶
0
40
80
120
160
200
240
280
(ev)

FIGURE 5

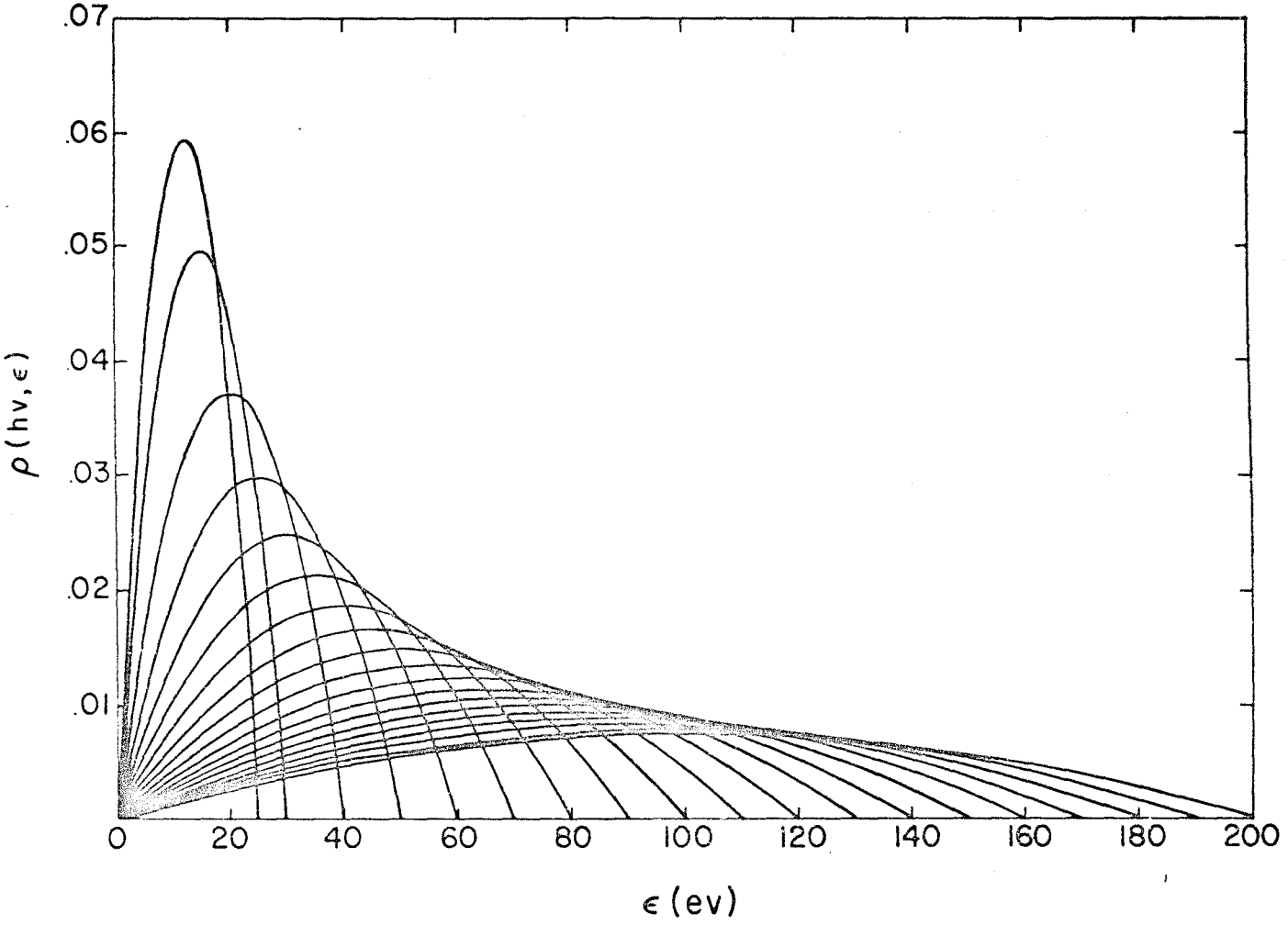

FIGURE 6

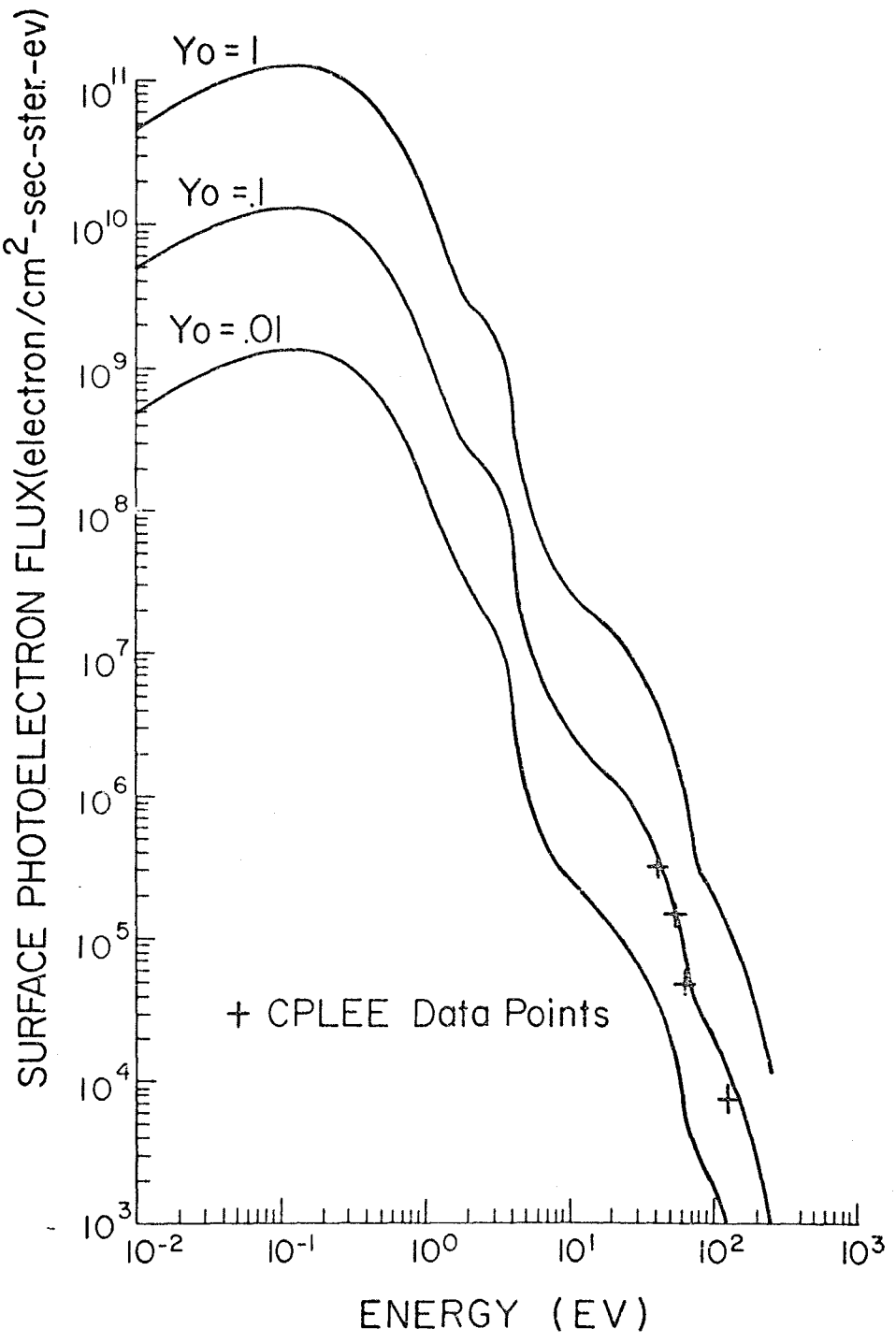
SURFACE PHOTOELECTRON FLUX(electron/cm^2-sec-ster.-ev)
Yo = 1
Yo = .1
Yo = .01
10^{11}
10^{10}
10^{9}
10^{8}
10^{7}
10^{6}
10^{5}
10^{4}
10^{3}
+ CPLEE Data Points
10^{-2}
10^{-1}
10^{0}
10^{1}
10^{2}
10^{3}
ENERGY (EV)

FIGURE 7

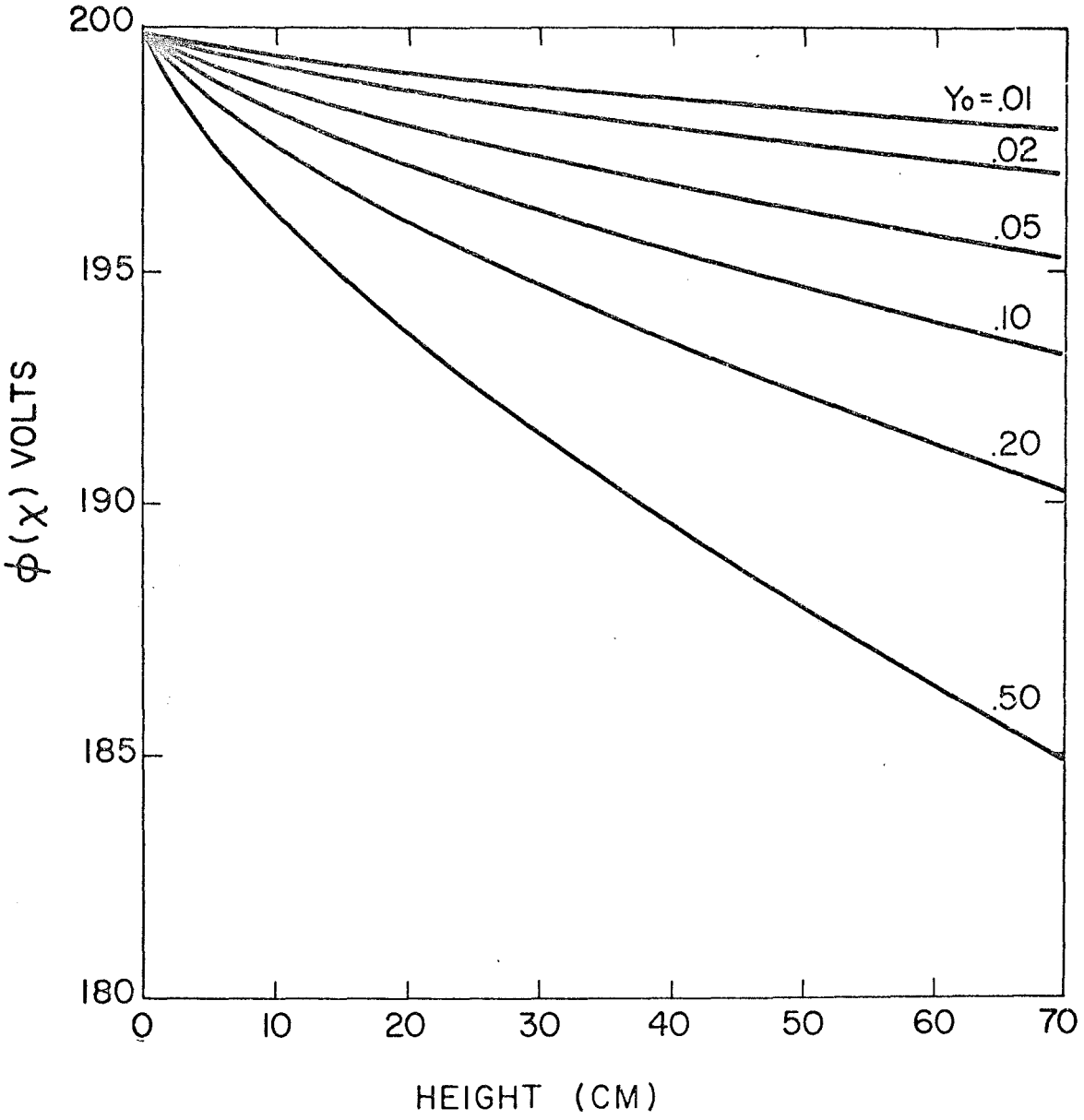
200
195
190
185
180
0
10
20
30
40
50
60
70
$\phi(\chi)$ VOLTS
HEIGHT (CM)
Y_0 = .01
.02
.05
.10
.20
.50

FIGURE 8

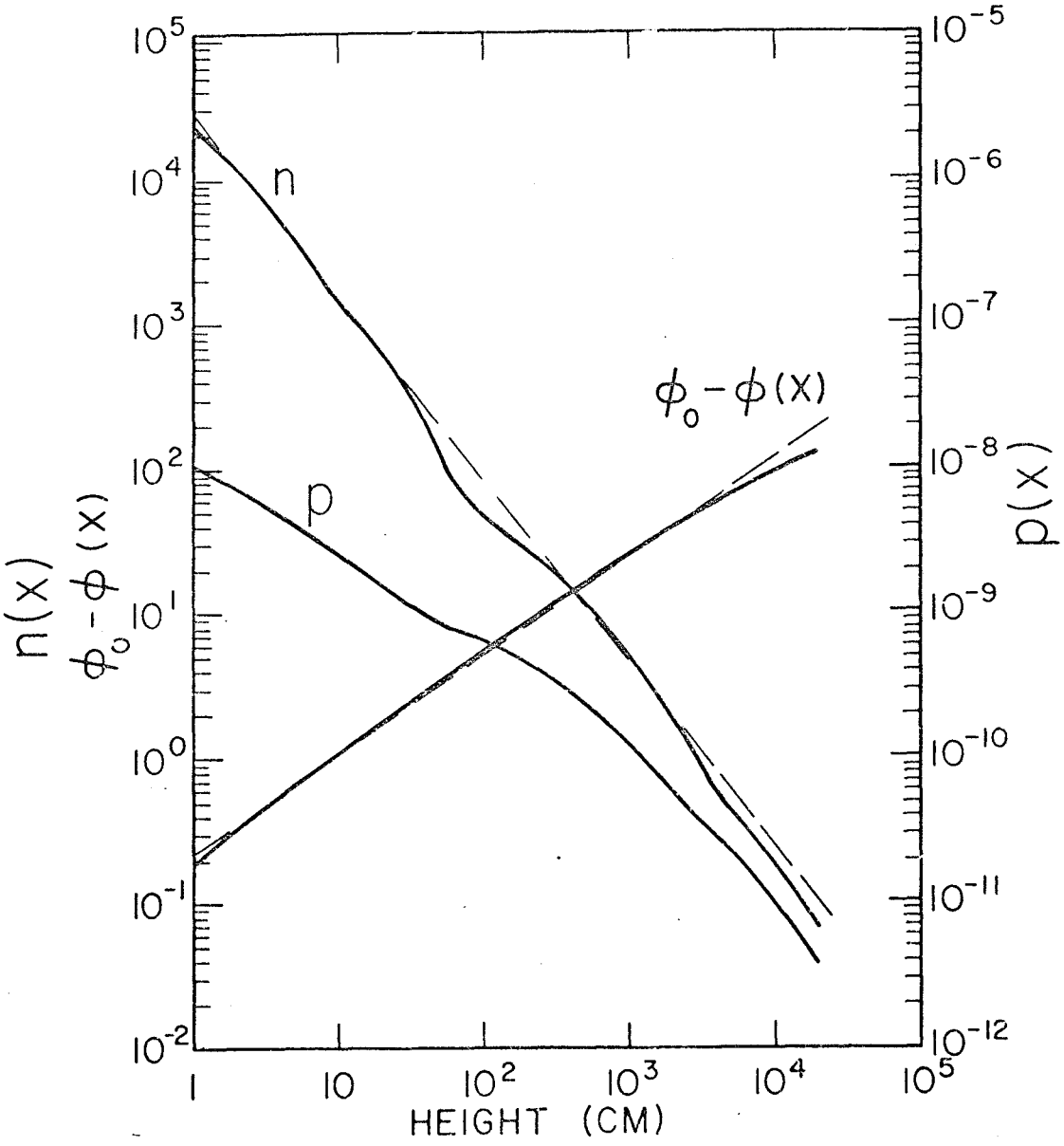
10^5
10^4
10^3
10^2
10^1
10^0
10^{-1}
10^{-2}
n
p
$\phi_0 - \phi(X)$
n(X)
$\phi_0 - \phi$ (X)
p(X)
10^{-5}
10^{-6}
10^{-7}
10^{-8}
10^{-9}
10^{-10}
10^{-11}
10^{-12}
1
10
10^2
10^3
10^4
10^5
HEIGHT (CM)

FIGURE 9

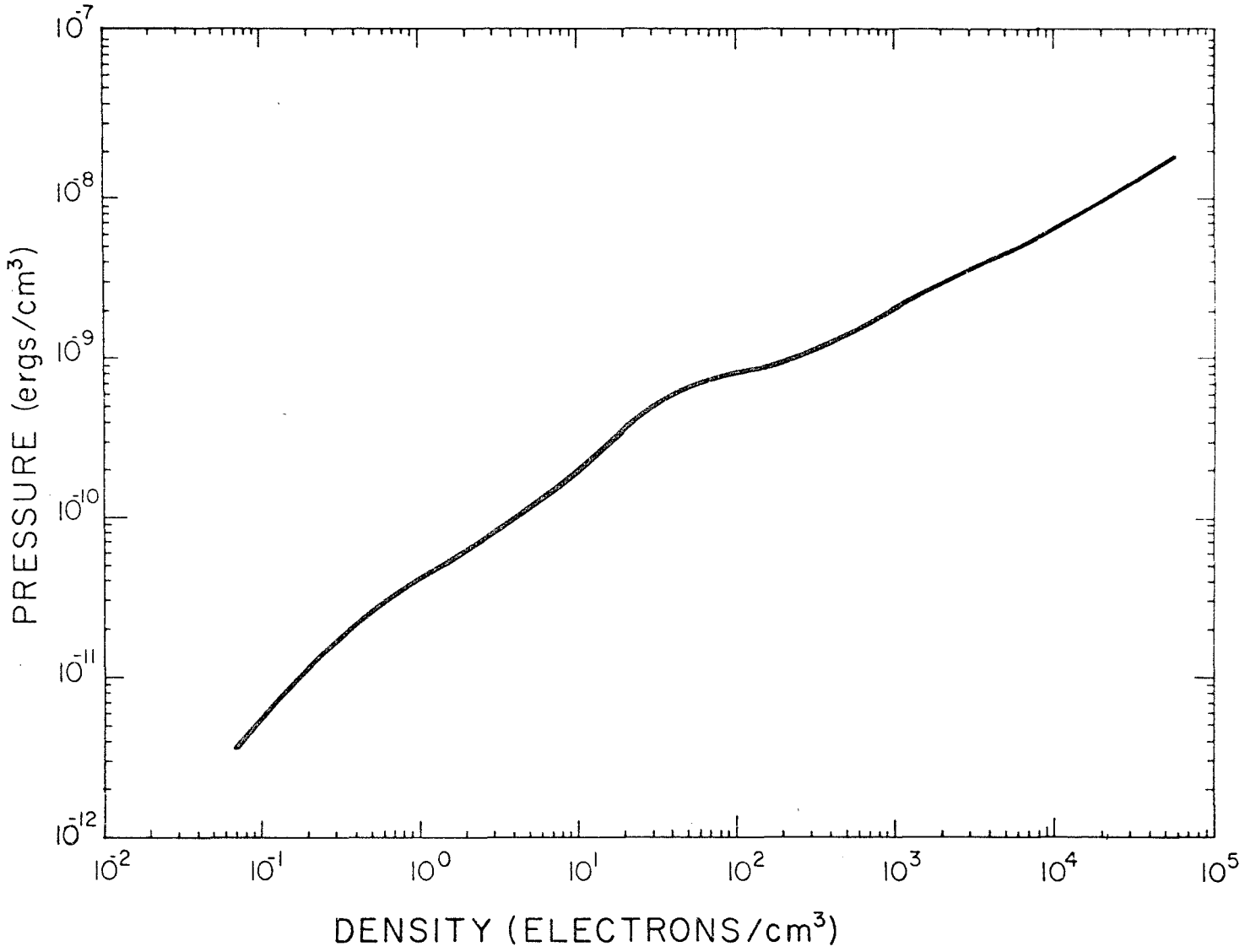
PRESSURE (ergs/cm³)
10⁻⁷
10⁻⁸
10⁻⁹
10⁻¹⁰
10⁻¹¹
10⁻¹²
10⁻²
10⁻¹
10⁰
10¹
10²
10³
10⁴
10⁵
DENSITY (ELECTRONS/cm³)

FIGURE 10